Cherenkov radiation emitted by ultrafast laser pulses and the generation of coherent polaritons

J. K. Wahlstrand and R. Merlin
FOCUS Center and Department of Physics, The University of Michigan, Ann Arbor, Michigan 48109-1120, USA
(Received 5 January 2003; revised manuscript received 20 May 2003; published 7 August 2003)

We report on the generation of coherent phonon polaritons in ZnTe, GaP, and $LiTaO_3$ using ultrafast optical pulses. These polaritons are coupled modes consisting of mostly far-infrared radiation and a small phonon component, which are excited through nonlinear optical processes involving the Raman and the second-order susceptibilities (respectively, impulsive stimulated Raman scattering and difference frequency generation). We probe their associated hybrid vibrational-electric field, in the THz range, by electro-optic sampling methods. The measured field patterns agree very well with calculations for the field due to a distribution of dipoles that follows the shape and moves with the group velocity of the optical pulses. For a tightly focused pulse, the pattern is identical to that of classical Cherenkov radiation by a moving dipole. Results for other shapes and, in particular, for the planar and transient-grating geometries are accounted for by a convolution of the Cherenkov field due to a point dipole with the function describing the slowly varying intensity of the pulse. Hence, polariton fields resulting from pulses of arbitrary shape can be described quantitatively in terms of expressions for the Cherenkov radiation emitted by an extended source. Using the Cherenkov approach, we recover the phase-matching conditions that lead to the selection of specific polariton wave vectors in the planar and transient grating geometry as well as the Cherenkov angle itself. The formalism can be easily extended to media exhibiting dispersion in the THz range. Calculations and experimental data for pointlike and planar sources reveal significant differences between the so-called superluminal and subluminal cases where the group velocity of the optical pulses is, respectively, above and below the highest phase velocity in the infrared. Using the Cherenkov radiation formalism, the fields generated by a spatiotemporally shaped pulse in a thick dispersive medium can be calculated analytically.

DOI: 10.1103/PhysRevB.68.054301 PACS number(s): 71.36.+c, 78.47.+p, 41.60.Bq

I. INTRODUCTION

Polaritons are hybrid modes of solids and, more generally, dense systems associated with elementary excitations that carry electromagnetic polarization.[1,2] Such excitations couple to light, resulting in a new mixed particle called the polariton. The polariton description is, in some sense, an alternative to that involving the index of refraction; polaritons are dressed photons. Phonon polaritons—lattice vibrations coupled to infrared light—were first studied experimentally by spontaneous Raman scattering.[3] Soon after, mixing of coherent polaritons with visible laser light was reported for GaP.[4] The generation, dispersion, and decay of phonon polaritons have been extensively investigated using various coherent optical methods, particularly coherent anti-Stokes Raman scattering (CARS) (Ref. 5) followed by time-domain CARS (Ref. 6) and, more recently, the closely related technique of impulsive stimulated Raman scattering (ISRS).

This work centers on ISRS: i.e., coherent scattering using pulses whose bandwidth exceeds the polariton frequency.[7] In ISRS experiments, a pump pulse imparts an impulsive force on the phonon component of the polariton, starting a coherent oscillation which in turn, through the inverse process, perturbs the index of refraction.[8,9] This perturbation is measured by a probe pulse that follows behind the pump pulse at a controllable time delay. The most common ISRS approach to generate coherent polariton fields is to use an intensity grating obtained from crossing two pump beams. This geometry leads to polaritons of nearly well-defined wave vector even in the pulsed case where the (transient) grating travels with the pulses.[10,11] An alternative method, associated with the nonlinear susceptibility $\chi^{(2)}$, is to excite the electromagnetic component of the polariton through difference frequency generation (DFG) or optical rectification.[12] Here, the pump pulse induces a nonlinear polarization proportional to its intensity envelope. If the pulse is tightly focused and its group velocity is greater than the phase velocity in the infrared, its polarization leads to emission of infrared light in much the same way that a relativistic dipole emits (coherent) Cherenkov radiation (CR). This interpretation, originally proposed for second-harmonic generation,[13] was put forth for DFG by Auston and co-workers[14–16] whose technique later became the standard for generating short THz pulses.[17] Recently, the CR interpretation was revisited in the analysis of pump-probe experiments on ZnSe (Ref. 18) and ZnTe (Ref. 19). In these and other polar materials, strong dispersion near the frequency of the transverse-optical (TO) phonon results in two qualitatively distinct regimes for CR depending on whether the velocity of the source is larger or smaller than the phase velocity of light at zero frequency. In the former, superluminal regime, the CR field is qualitatively the same as in the experiments of Auston and Nuss[16] whereas the latter subluminal regime displays new features.[20]

To our knowledge, there does not exist a clear, unified discussion in the literature of the relationship between the transient grating and tightly focused single-pump methods. While the generation mechanisms are identical, ISRS is often described in a four-wave mixing framework and, as such, as a technique that distinguishes itself from DFG. Here, we present a unified discussion of the two methods based on the CR picture, showing that the generation of THz radiation by single or multiple pulses of arbitrary shape can always be

described as CR. We also report experimental results on three materials: ZnTe, GaP, and $LiTaO_3$ in three geometries (point, planar, and transient grating) using an electro-optic field sampling technique based on that of Auston and Nuss.[16] This method allows us to map out the polariton field as a function of time delay and lateral position for polarization sources of arbitrary shape and, simultaneously, to image the shape of the source pulse itself.

II. PHONON POLARITONS AND OPTICAL SUSCEPTIBILITIES

As mentioned earlier, polaritons can be described either as excitations that carry polarization through the coupling to the electromagnetic field or as light perturbed by the refractive index of the medium, which exhibits strong dispersion near the resonant TO frequency. In the Cherenkov picture of phonon polariton generation we take the latter view, incorporating the effect of the infrared-active phonon into the dielectric function and the second-order nonlinear susceptibility. For a diatomic cubic lattice and neglecting damping, the dielectric function is of the Lorentz form

$$\epsilon(\Omega)=\epsilon_\infty+\frac{\epsilon_0-\epsilon_\infty}{1-(\Omega/\Omega_{\mathrm{TO}})^2}, \tag{1}$$

where Ω_{TO} is the TO frequency of the threefold-degenerate infrared-active mode, ϵ_∞ is the dielectric constant including the effects of higher-lying resonances, and ϵ_0 is the static dielectric constant. The Lyddane-Sachs-Teller (LST) formula $\Omega_{\mathrm{LO}}^2=(\epsilon_0/\epsilon_\infty)\Omega_{\mathrm{TO}}^2$ gives the relationship between Ω_{LO}, the longitudinal optical (LO) phonon frequency, and Ω_{TO}. The refractive index $n(\Omega)=\sqrt{\epsilon(\Omega)}$, phase velocity $c/n(\Omega)$, and polariton dispersion relation $\Omega=cq/n(\Omega)$ are plotted in Fig. 1 for a material with $\epsilon(\Omega)$ given by Eq. (1). In this work we deal mainly with frequencies below Ω_{TO}. Near zero frequency, where the dispersion curve is linear, the polariton is mostly light like whereas, near Ω_{TO}, it is phonon like. When there is more than one infrared-active phonon, as in $LiTaO_3$, each mode contributes to the polarization and the dielectric function reflects a sum of these contributions (poles).

The nonlinear interaction of visible light with phonon polaritons involves both the lattice and THz electromagnetic field. The nonlinear tensor that couples polaritons and visible light is thus composed of two parts: the Raman tensor $d\chi/dQ=\chi^{\mathrm{R}}$, which couples visible light to the phonon mode with amplitude Q, and the second-order nonlinear susceptibility $d\chi/dE=\chi^{(2)}$, which couples visible to infrared electric fields. Both of these susceptibilities are almost entirely electronic in nature. Counting both contributions, the total nonlinear polarization is[4]

$$P_i^{\mathrm{NL}}=\chi_{ijk}^{(2)}E_j(\Omega)E_k(\omega_L)+\chi_{ik}^{\mathrm{R}}Q_jE_k(\omega_{\mathrm{L}}), \tag{2}$$

where Q_j is the amplitude of one of the threefold-degenerate phonon modes, ω_L is the frequency of the visible laser light, and Ω is the frequency of the phonon polariton. As is well known, the Raman contribution can be included in an effective nonlinear susceptibility d_{ijk}, each tensor element of which is of the form

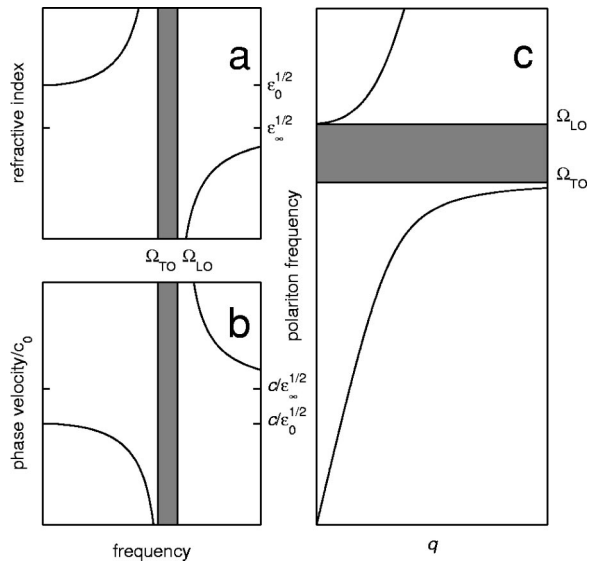

FIG. 1. Optical parameters for a generic material with a single triply degenerate infrared-active phonon; see Eq. (1). (a) Refractive index n, (b) phase velocity c/n, and (c) polariton dispersion. The darkened regions indicate the band between Ω_{TO} and Ω_{LO} in which light cannot propagate.

$$d(\Omega)=\chi^{(2)}\left[1+C\left(1-\frac{\Omega^2}{\Omega_{\mathrm{TO}}^2}\right)^{-1}\right], \tag{3}$$

where the Faust-Henry coefficient $C=\chi^{\mathrm{R}}(\chi^{(2)})^{-1}e^*\mu^{-1}(\Omega_{\mathrm{TO}})^{-2}$ gives the ratio of the Raman (often termed ionic) to electronic contribution.[4] Here, e^* is the transverse effective charge and μ is the reduced mass of the lattice mode. Because χ^{R} and $\chi^{(2)}$ do not change appreciably with frequency in the THz range, C can be approximated as a constant for a given laser wavelength and material. If there is more than one phonon mode, there is a Raman contribution to d and to the Faust-Henry coefficient from each one. In our experiments we do not need to consider the dispersion of d, for we mainly deal with low-frequency polaritons. Thus, in the following we assume that the nonlinear susceptibility is constant and approximately given by $\chi^{(2)}(1+C)$.

III. THEORY OF CHERENKOV EMISSION IN AN INFINITE CRYSTAL

In noncentrosymmetric media, an optical pulse induces through $\chi^{(2)}$ a low-frequency polarization proportional to its intensity. This is DFG, also known as optical rectification.[12] The dipolar charge distribution moves at the optical pulse's group velocity v_{g} and, like a charged particle, it can emit CR if v_g is greater than the phase velocity of the THz radiation in the medium. The bandwidth of the THz radiation emitted by a pulse is limited to the pulse bandwidth. The spatial and temporal shapes of the pulse envelope, together with the op-

tical properties of the medium, determine the THz field.

Kleinman and Auston adapted the theory of CR to an optical pulse traveling through a nonlinear isotropic medium.[15] Their approach, which we build on here, is essentially to separate the nonlinear mechanism by which the polarization in the medium is generated from the Cherenkov mechanism by which infrared light is emitted. This approach works well in the absence of higher-order effects such as self-focusing and self-phase modulation, which affect the spatiotemporal shape of the pulse as it propagates, and depletion, which diminishes the induced polarization. Neglecting these effects, the emission process is entirely analogous to the emission of CR by a continuum of dipoles traveling at the group velocity of the pulse. In the following, we discuss electro-optic CR by pulses of a variety of spatiotemporal shapes.

A. Point source

For a beam focused to a small waist compared to the polariton wavelength, the polarization induced by the optical pulse can be approximated by a point dipole. This geometry, the three-dimensional (3D) case discussed by Kleinman and Auston,[15] is the closest electro-optic analog to conventional CR (emitted by a relativistic monopole), which is coherent. The theory of CR was largely worked out more than 60 years ago by Tamm and Frank.[21,22] For an infinite medium and pulses propagating along the z axis, the fields are a function of $z-v_g t$ and the cylindrical coordinates ρ and ϕ. This approximation, valid for a thick sample, greatly simplifies the theory.

The radiation field due to a propagating dipole can be derived from the radiation field due to a monopole by taking a derivative in the direction of the dipole orientation.[23] In the experiments discussed here, the induced dipole is oriented perpendicular to the z axis. For this orientation, the fields are proportional to $\cos\phi$, where ϕ is measured from the direction of the dipole; dropping for simplicity the ϕ dependence, we have[21–23]

$$E_z(\rho,z-v_g t)\propto\int e^{i\Omega(t-\frac{z}{v_g})}\left(\frac{c^2}{v_g^2 n^2(\Omega)}-1\right)\frac{\partial a}{\partial\rho}\Omega d\Omega, \tag{4}$$

$$E_\rho(\rho,z-v_g t)\propto\int -ie^{i\Omega(t-z/v_g)}\frac{1}{n^2(\Omega)}\frac{\partial^2 a}{\partial\rho^2}d\Omega, \tag{5}$$

where E_z and E_ρ are the z and ρ components of the electric field and

$$a(\rho,\Omega)=H_0^{(1)}[s(\Omega)\rho], \tag{6}$$

where $H_0^{(1)}$ is a Hankel function and $s(\Omega)=\Omega(\epsilon v_g^2/c^2-1)^{1/2}/v_g=\Omega\tan\theta_C/v_g$.

Radiation is emitted at frequencies for which the Cherenkov condition $v_g>c/n(\Omega)$ is satisfied. Integrating Eq. (5) over these frequencies, two qualitatively different radiation patterns emerge, depending on v_g.[24] For $v_g>c/n(0)$, the laser pulse propagates faster than the entire lower polariton branch $0<\Omega<\Omega_{\mathrm{TO}}$. We call this the superluminal regime. For $v_g<c/n(0)$, the laser pulse only travels faster for frequencies in the band $\Omega_C<\Omega<\Omega_{\mathrm{TO}}$, where the velocity-matched frequency Ω_C is defined by $v_g=c/n(\Omega_C)$. We have referred to this as the subluminal regime.[25]

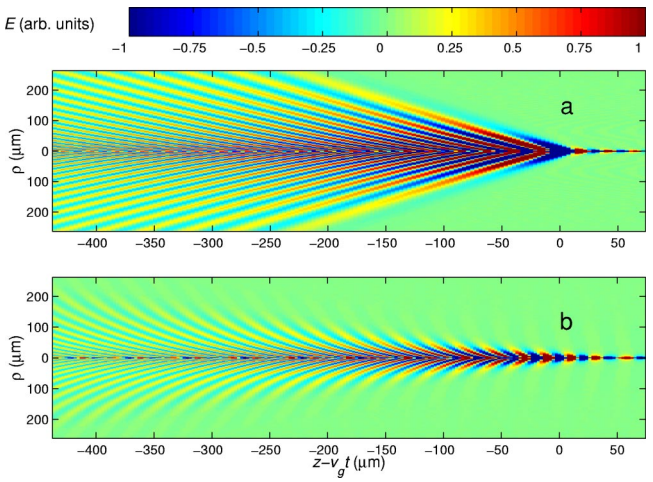

FIG. 2. (Color online) Calculated E_ρ for a point dipole at $\rho=0$ and $z-v_g t=0$ traveling through a medium with dispersion given by Eq. (1). (a) Superluminal, $v_g>c/n(0)$, and (b) subluminal, $v_g<c/n(0)$, regimes.

Shown in Fig. 2 are plots of E_ρ, calculated using Eq. (5), in a medium with refractive index given by Eq. (1). For the superluminal regime [Fig. 2(a)], there is a sharp shock front with small-amplitude ripples behind it. The weak ripples are due to dispersion, but the shock wave is defined by $\Omega=0$. On the other hand, the subluminal regime [Fig. 2(b)] is dominated by dispersion effects. The angle of the phase front depends on ρ, and there is a large field near the axis of motion $\rho=0$. The radiation pattern is still confined within a cone, but the cone angle becomes larger as v_g decreases, in contrast to the superluminal regime. The special features of the subluminal regime are apparent in the calculations reported by Afanasiev and co-workers.[20]

In the CR literature, it is common to use the asymptotic form of the fields for large ρ to find an approximate analytical solution. In this limit, E_ρ becomes

$$E_\rho\propto\int_{\Omega_C}^{\Omega_{\mathrm{TO}}}\frac{i\sqrt{2s^3(\Omega)}}{n^2(\Omega)\sqrt{\pi\rho}}e^{-i[\Omega(t-z/v_g)-s(\Omega)\rho+\pi/4]}d\Omega. \tag{7}$$

For large ρ, the integral is small except for values of Ω for which the integrand does not oscillate. Using the stationary phase method, Eq. (7) can be approximated as

$$E_\rho\propto\sum_{\Omega_i}\frac{2\sqrt{s^3(\Omega_i)}}{n^2(\Omega_i)\rho}\frac{1}{\sqrt{|s''(\Omega_i)|}}e^{-i[\Omega_i(t-z/v_g)-s(\Omega_i)\rho]}, \tag{8}$$

where Ω_i are the frequencies within the range of integration for which the phase in the exponential is stationary. These are the solutions to

$$v_g\frac{ds}{d\Omega}=\frac{v_g t-z}{\rho}=\cot\theta, \tag{9}$$

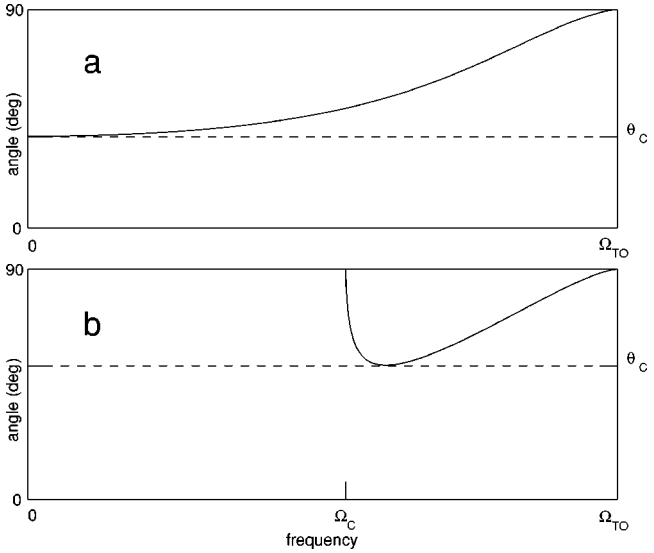

FIG. 3. Plot of angle vs polariton frequency; see Eq. (10). The dashed line indicates the Cherenkov angle θ_C, and Ω_C indicates the group-velocity-matched frequency. (a) Superluminal regime. (b) Subluminal regime.

which defines a cone of angle θ with respect to the z axis. The cone angle depends on frequency because $s(\Omega)$ contains $n(\Omega)$. Explicitly, Eq. (9) becomes

$$v_g \frac{ds}{d\Omega} = \Omega^2 \frac{v_g}{sc^2} \frac{d\epsilon}{d\Omega} + \frac{v_g s}{\Omega} = \cot\theta. \tag{10}$$

The dependence of θ on Ω is plotted for the two regimes in Fig. 3. In the superluminal case [Fig. 3(a)], θ is a monotonic function of frequency, whereas in the subluminal regime [Fig. 3(b)] two frequencies map onto the same angle, resulting in the complex beating behavior shown in Fig. 2(a).

The angle θ_C, defined as the smallest angle at which radiation is emitted, is shown as a dashed line in Fig. 3. The frequencies associated with this angle are solutions to $s''(\Omega)=0$. In the superluminal regime, $\epsilon(\Omega)v_g^2/c^2-1>0$ for all frequencies within the range of integration, and $\Omega=0$ is the only solution. Thus, from Eq. (10), $\cos\theta_C = v_g n(0)/c$, which is the standard Cherenkov formula. In the subluminal regime, there are two solutions. For a material with dispersion given by Eq. (1), $\theta_C = \tan^{-1}(4\gamma^{-1}\sqrt{(\eta-\zeta)/\zeta^3})$, where $\gamma=(1-\epsilon_\infty v_g^2/c^2)^{-1/2}$, $\zeta = 2-(4-3\eta)^{1/2}$, and $\eta=1-(\Omega_C/\Omega_{\rm TO})^2$.[20]

So far, we have considered isotropic materials, and therefore, the considerations above apply to ZnTe and GaP but, in the strictest sense, not to the uniaxial $LiTaO_3$. The theory of CR in an anisotropic material is considerably more complex than that discussed here, because extraordinary and ordinary waves may be emitted. Other complications result for the case of an extremely tightly focused pulse, for which there exists a small longitudinal component of the laser electric field, leading to the breakdown of the point dipole approximation. In addition, the confocal parameter comes into play, resulting in the breakdown of the infinite crystal approximation. We note in passing that exact integrals for an electric dipole oriented arbitrarily with respect to the axis of motion, as well as those of a magnetic dipole, are given in the work of Zrelov.[23]

B. Planar source

When the beam waist w is much larger than the wavelength of the polariton ($w \gg 2\pi cn/\Omega$), we have another important limiting case. Here, the polarization induced by the optical pulse is shaped like a pancake. This planar geometry is often used for the generation and detection of THz pulses by nonresonant optical rectification.[26,27]

For an infinitely thick crystal and approximating the optical pulse as infinitely short (this is valid as long as the pulse is short compared to the period of the radiation being generated), the polarization induced is $\mathbf{P} \approx \zeta \delta(z-v_g t)\mathbf{e}_d$, where $\mathbf{e}_d$ is a unit vector pointing in the direction of the dipole orientation and ζ is the areal polarization. It is possible to obtain the CR field from the point dipole solution by convolution, but here we use the corresponding Hertz potential

$$\mathbf{\Pi}(\Omega) = -\frac{4\pi\zeta e^{-i\Omega(t-z/v_g)}}{v_g \epsilon(\Omega) s^2(\Omega)} \mathbf{e}_d. \tag{11}$$

The electric field is then[18]

$$\mathbf{E} = \int_0^{\Omega_{\rm TO}} \frac{\epsilon(\Omega)\Omega^2}{c^2} \mathbf{\Pi}(\Omega) d\Omega \tag{12}$$

$$= -\frac{4\pi\zeta}{v_g c^2} e_d \int_0^{\Omega_{\rm TO}} \frac{\Omega^2 e^{-i\Omega(t-z/v_g)}}{s^2(\Omega)} d\Omega. \tag{13}$$

It can be shown that the field vanishes unless $s^2(\Omega)=0$. In the superluminal regime, $s^2(\Omega)>0$ for all Ω, and $\mathbf{E}=0$. In the subluminal regime, $s^2(\Omega_C)=0$. Note that the phase matching condition is *only* met in the presence of dispersion. In the superluminal regime, no radiation is emitted from the bulk because the pulse is traveling faster than the phase velocities of all infrared frequencies.

Practically, a beam cannot be focused to a point; nor is it really planar. If cylindrical lenses are used to focus the beam, it can be extended in one direction and tightly focused in another. The extreme case of the 2D geometry was treated by Kleinman and Auston.[15] The point geometry solution is the Green's function of the problem, in that the radiation pattern of an arbitrary source can be obtained by convolution of the point solution with the source shape. Two examples are shown in Fig. 4. This convolution technique is potentially useful for calculating the THz field generated in a thick subluminal crystal by a spatially extended source because it quantifies phase-matching issues encountered due to dispersion in the infrared. In addition, it is a powerful machinery for calculating the radiation field generated by ultrafast optical pulses which have been shaped spatially and temporally—for example, in the manner recently demonstrated by Koehl, Adachi, and Nelson.[28] To the best of our knowledge, our approach has not been previously applied to this problem.

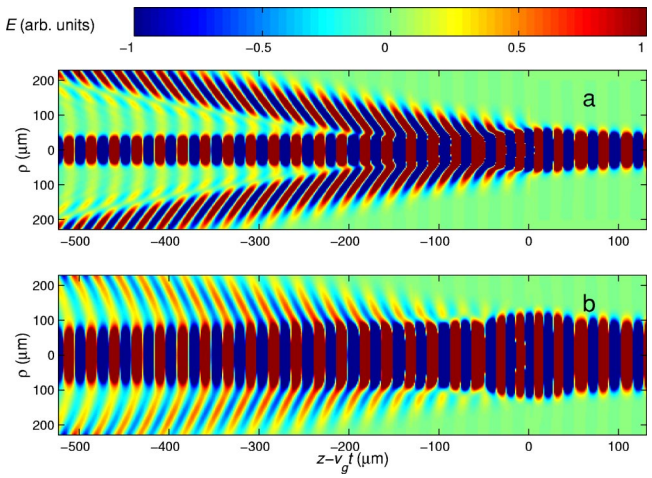

FIG. 4. (Color online) Calculated E_ρ for an extended source of width w, obtained by convoluting results for a point dipole with a Gaussian in the ρ direction (subluminal regime). (a) $w=20$ μm, (b) $w=40$ μm.

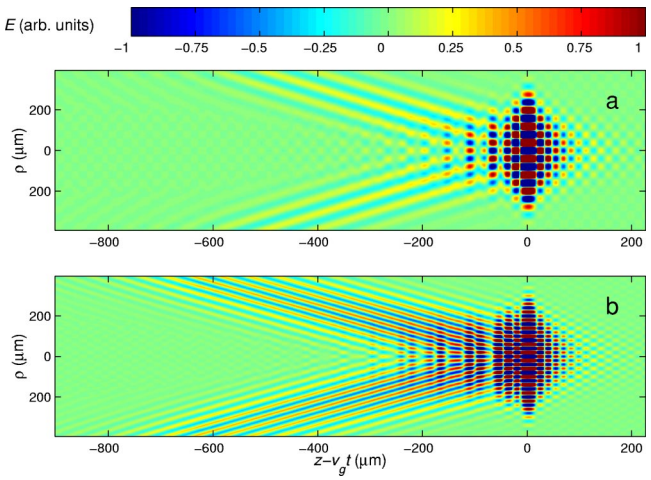

FIG. 5. (Color online) Calculated E_ρ due to a transient grating, showing the checkerboard polariton field pattern generated behind the grating. The grating wave vector in (a) is smaller than in (b).

C. Periodic source (transient grating)

The last source shape we consider is a periodic distribution, or transient grating, implemented by interfering two pump beams inside the sample. This geometry is useful because it excites a unique polariton wave vector determined by the grating period. If we cross two pump beams of equal intensity at an angle α, Gaussian in space with waists w_x in the x direction and w_y in the y direction and Gaussian in time with pulse width τ, the intensity grating has the form

$$I(x,y,z-v_g t)\propto e^{-x^2/w_x^2-y^2/w_y^2}\cos\left(\frac{k_L x}{\sin\alpha}\right)e^{-(z/v_g-t)^2/\tau^2}, \tag{14}$$

where k_L is the wave vector of the laser light inside the medium. Here, we have assumed that α is small, which makes v_g approximately equal to the group velocity of each separate pulse. This is a good approximation for the experiments described here, since k_L is much larger than the wave vector of the gratings. The Cherenkov angle converts the spatial periodicity of the transient grating into a temporal periodicity in the polariton field, resulting in a checkerboard pattern and a well-defined polariton frequency Ω, as shown in Fig. 5.

In the impulsive limit, a defocused probe pulse traveling at the same speed as the pump pulse and, thus, at the speed of the polariton field samples a slice of the checkerboard field in the xy plane. The electric field in this slice is periodic with the same wave vector $k_x=k_L/\sin\alpha$ as the intensity grating. Through the electro-optic effect, the probe pulse diffracts from the periodically varying index of refraction, resulting in an oscillatory signal at 2Ω as a function of time delay, because the diffracted intensity is proportional to $|E|^2$. This technique is known as homodyne detection in the ISRS literature.[10] Heterodyne detection,[11,29,30] in which one mixes the diffracted signal with undiffracted probe light, gives a much larger signal at Ω, because the signal is proportional to E. Because it is sensitive to the phase of the polariton field, which defines the phase of the diffracted probe pulse, heterodyne detection works just as well outside the checkerboard, in what we might call the Cherenkov wing of the field. As we discuss in detail below, heterodyne detection is often discussed in terms of four-wave mixing.[29]

It is important to emphasize that the wave vector of the grating is not the same as the polariton wave vector, since the polariton propagates in the direction normal to the wave front. The magnitude of the polariton wave vector is given by $q=k_x\sin\theta$, where θ is the Cherenkov angle. In many early ISRS papers, it is assumed that the wave vector of the grating is the same as the polariton wave vector, tantamount to assuming that θ is very large. This is generally a poor approximation and leads to incorrect polariton dispersion measurements, as recently pointed out by Hebling.[31]

The simple interpretation above works best for large w_x, in which case the polariton wave vector is well defined. For small w_x, edge effects make the polariton field more complex but, by convolving the point dipole solution with the grating (as in Fig. 5), we can calculate the polariton field due to a grating of arbitrary shape.

IV. PHASE MATCHING

One potential source of confusion when comparing the transient grating, tightly focused, and planar geometries is that, at first glance, the phase-matching conditions seem entirely different, especially the hidden role of the pulse's group velocity in the transient-grating geometry. Here we discuss phase matching in all three geometries in a unified manner based on CR. An ultrafast pulse contains a continuum of frequencies and wave vectors, and the generated polariton wave vectors are determined by conservation of energy and momentum. The Cherenkov interpretation is, of course, consistent with phase matching. In all geometries, the nonlinear polarization contains terms of the form $e^{i(\mathbf{k}_2-\mathbf{k}_1)\cdot\mathbf{r}-i(\omega_2-\omega_1)t}$, where $\mathbf{k}_1$, $\mathbf{k}_2$, ω_1, and ω_2 denote wave vector and frequency components of the optical pulse. For the planar geometry, the wave vector components all

point along the z axis, and conservation of momentum requires $q=k_2-k_1=[\omega_2 n(\omega_2)-\omega_1 n(\omega_1)]/c$, where q is the polariton wave vector. Since $\Omega=\omega_1-\omega_2$,

$$q=\frac{\omega_2 n(\omega_2)-(\omega_2+\Omega)n(\omega_2+\Omega)}{c} \tag{15}$$

$$\approx\frac{\Omega}{c}[n(\omega_2)+\omega_2 n'(\omega_2)]=\frac{\Omega}{v_g(\omega_2)}, \tag{16}$$

making the connection to the group-velocity-matching argument derived in Sec. IIIB.

A tightly focused optical pulse has wave vector components pointing in many directions. The dependence of the polarization on $z-v_g t$ forces $q_z=\Omega/v_g$. The polariton wave vector and frequency must also satisfy $\Omega=|\mathbf{q}|c/n(\Omega)$. Let q_ρ be the component of the polariton wave vector perpendicular to the z axis. Momentum conservation gives

$$\frac{q_\rho}{q_z}=\frac{\sqrt{q^2-q_z^2}}{\Omega/v_g}=\sqrt{\frac{n^2(\Omega)v_g^2}{c^2}-1}, \tag{17}$$

and the polariton is emitted at an angle $\tan^{-1}q_\rho/q_z$ to the z axis, which is identical to the Cherenkov angle.

In the transient-grating geometry, the angle between $\mathbf{k}_1$ and $\mathbf{k}_2$ is well defined, and the wave vector $\mathbf{q}=\mathbf{k}_1-\mathbf{k}_2$ is emitted in the direction given by Eq. (17) because the polarization is a function of $z-v_g t$. The transient-grating configuration allows one to excite wave vectors that are higher than those accessible in the planar geometry.

A recently proposed technique developed by Hebling and co-workers relies on a tilted pulse front.[32] This can also be encompassed in a Cherenkov radiation framework as a planar source which propagates at an angle. Tuning the tilt angle changes the wave vector of the generated polariton, and this shows promise as an easily tunable THz source.

As is well known, it is possible to interpret ISRS as a $\chi^{(3)}$ process.[29] Here one hides both the generation and detection of the polariton in $\chi^{(3)}_{\rm eff}$, much as we included the Raman contribution to the generation of the polariton in $\chi^{(2)}$. The polarization is

$$\begin{aligned}P(\omega_s)&=\chi^{(3)}_{\rm eff}(\omega_p,\Omega-\omega_p,\omega_p)E_1(\omega_1)E_2^*(\omega_1-\Omega)E_p(\omega_p)\\&=d(\Omega)[d(\Omega)E_1(\omega_1)E_2^*(\omega_1-\Omega)]E_p(\omega_p),\end{aligned} \tag{18}$$

where E_1 and E_2 are the pump fields, E_p is the probe field, and d is the effective nonlinear susceptibility defined in Sec. II. All propagation and damping effects can be included in $\chi^{(3)}_{\rm eff}$, and this formalism is often used.[6]

Finally, we discuss briefly the advantages and disadvantages of the various scattering geometries. The experiments with tightly focused beams produce the highest peak polariton amplitude (for a given pulse peak power), but also a wide range of wave vectors and frequencies. ISRS by a transient grating has the advantage of defining the polariton wave vector and producing a large-amplitude polariton at that particular wave vector. CARS has the advantage of yielding the best frequency and wave vector resolution.

TABLE I. Parameters used in the calculations.

Parameter	GaP	ZnTe	$LiTaO_3$ [a]
$\Omega_{TO}/2\pi$ (THz)	11.0[b]	5.32[c]	6[d]
$\Omega_{LO}/2\pi$ (THz)	12.1[b]	6.18[c]	12[e]
$\sqrt{\epsilon_0}$	3.31[f]	3.16[c]	6.3[d]
n_g at 800 nm	3.56[f]	3.24[g]	2.2
$\Omega_C/2\pi$ [h](THz)	7.7	2.2	-

[a]Parameters are for the lowest A_1 mode.
[b]Reference 33.
[c]Reference 34.
[d]Reference 35.
[e]From LST relation using parameters of Ref. 35.
[f]Reference 36.
[g]Reference 37.
[h]Calculated from ϵ_∞.

V. MATERIALS

Generation of electro-optic CR requires a nonzero $\chi^{(2)}$, present only in crystals without inversion symmetry. In our experiments, we used three readily available and well-characterized materials: the zinc-blende ZnTe and GaP, and the perovskite $LiTaO_3$. The parameters relevant to our work are listed in Table I.

A. GaP and ZnTe

Materials with the zinc-blende structure have a triply degenerate infrared-active optical mode. For light normally incident on a (110) face, the selection rules forbid excitation of the nondispersive LO mode. For the TO mode,

$$R_1=\begin{pmatrix}0&0&-b\\0&0&b\\-b&b&0\end{pmatrix}\quad R_2=\begin{pmatrix}0&b&0\\b&0&0\\0&0&0\end{pmatrix}, \tag{19}$$

where R_1 and R_2 are the Raman tensors for the modes polarized along the $[1\bar{1}0]$ and [001] directions, respectively. The single independent tensor component b corresponds to the nonlinear coefficient d_{41}. The dipolar distribution induced by the pump pulse is always oriented perpendicular to the [110] direction. We measure the polariton by the inverse process, and we are only sensitive to the electric field component E_ρ.

In their pioneering work using nonlinear mixing of visible and infrared cw laser light, Faust and Henry measured $C=-0.47$ in GaP.[4] This leads to total destructive interference between the ionic and electronic contributions to d at 6.5 THz. Because this frequency is close to Ω_C for Ti:sapphire pulses, this results in a small signal. Recently Leitenstorfer and co-workers found $C=-0.07$ in ZnTe by analyzing data from time-domain spectroscopy of THz pulses by electro-optic sampling.[38] This small value leads to $d=0$ at 5.2 THz, very close to Ω_{TO}. For our experiment in ZnTe, we are only able to measure up to roughly 4 THz, not high enough to probe effects of the dispersion of d.

B. $LiTaO_3$

This material crystallizes in the perovskite structure. $LiTaO_3$ is ferroelectric at room temperature and exhibits four A_1 symmetry and nine E symmetry modes, all of which are Raman and infrared active.[39] There has been considerable disagreement over the assignment of several Raman peaks, but the lowest-frequency A_1 mode considered here is well characterized. The Raman tensor for A_1 phonons is[39]

$$A_1 = \begin{pmatrix} a & 0 & 0 \\ 0 & a & 0 \\ 0 & 0 & b \end{pmatrix}. \tag{20}$$

The independent tensor elements a and b are associated with the nonlinear coefficients d_{31} and d_{33}, respectively. Here, we use $\chi^{(2)}=d_{33}$ and $\chi^{\mathrm{R}}=b$, which are the largest coefficients, to both generate and detect the polariton. The dipolar distribution points along the optic axis, and the probe pulse is sensitive to the component of the Cherenkov electric field along that axis. Barker, Ballman, and Ditzenberger measured the infrared reflectivity and found that, for the extraordinary index, most of the oscillator strength in the infrared is in the lowest-lying A_1 TO mode.[35] This mode is also the strongest Raman scatterer. We performed our experiment on the lowest polariton branch.

The refractive index in the visible is weakly anisotropic. Since the laser pulses in our experiment are polarized along the optic axis, there is no effect of this anisotropy, in contrast with experiments on E modes.[40] The static dielectric constant is also weakly anisotropic. However, since the lowest-lying A_1 and E TO frequencies are different (6 and 4.2 THz, respectively), the dielectric function becomes more anisotropic at large frequencies, where the cubic approximation is expected to break down. For the low frequencies discussed here, the approximation is well obeyed. For the lowest-lying A_1 mode in $LiTaO_3$, C is positive.[41]

VI. EXPERIMENTS

A. Techniques

Our experimental technique is similar to that of Auston and Nuss.[16] A diagram of the experimental setup is shown in Fig. 6. Pump and probe beams are focused and crossed inside the sample. The pump pulse is the Cherenkov source and the tightly focused probe serves as the detector of the Cherenkov radiation field. The probe pulse ''surfs'' on top of the Cherenkov wakefield generated by the pump pulse and samples the polariton field through both the linear electro-optic and the Raman effects, which both cause changes in the refractive index. We change the time delay (t) between pump and probe with a motorized delay stage in the probe path and the relative focal position (ρ) between pump and probe by moving a motorized translation stage upon which the pump's focusing lens is mounted. By sampling the diffracted probe beam as a function of t and ρ, we map the polariton field.

We used two different detection schemes. The first is a frequency shift measurement, which takes advantage of the

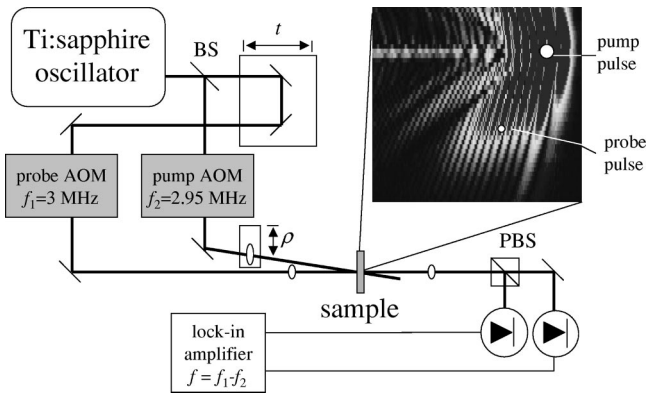

FIG. 6. Experimental setup. Pulses split into pump and probe beams; the time delay t between the pulses is varied with an automated translation stage. The relative position of the two beams ρ is adjusted by moving a single lens. The inset shows a close-up of the geometry inside the crystal. The pump and probe pulses travel along parallel paths inside the crystal at the same group velocity v_g. BS and PBS denote, respectively, a 10:1 beam splitter and a polarizing beam splitter. Not shown are $\lambda/2$ waveplates, used to rotate the polarization of the pump and probe beams, and a $\lambda/4$ waveplate in the probe path which resolves the induced birefringence due to the electro-optic effect.

fact that the spectrum of the probe is shifted proportional to dn/dt.[8] The polariton induces a change in the index of refraction due to its electromagnetic and vibrational components, so that dn/dt contains terms proportional to dE/dt and dQ/dt. We measure the frequency shift by cutting half of the probe spectrum with a bandpass filter before detection with a photodiode. This technique is especially useful when the pump and probe polarizations are chosen perpendicular to each other to suppress the scattered pump light. The second technique, widely used for detecting THz radiation, is polarization detection.[26,42] When properly oriented, the polariton's electric field induces birefringence, which can be probed by measuring the polarization state of the probe beam after the sample. This yields a signal directly proportional to the THz Cherenkov electric field.

The spot size inside the crystal was determined experimentally using the same technique. In ZnTe and GaP, two-photon absorption depletes the probe when pump and probe overlap temporally and spatially, creating a large Gaussian peak in the signal. In $LiTaO_3$, the intensity-dependent refractive index due to $\chi^{(3)}$ modulates the probe pulse's phase when it overlaps with the pump pulse, also producing a large signal (known as the coherent artifact).

Auston and Nuss used thin samples and a collinear geometry to achieve spatial resolution on the order of 1.5 μm.[16] A problem with this setup is that it is difficult to measure the field behind the source, because of strong pump scattering due to the fact that the two beams are collinear. In order to measure the source itself plus the field behind it, we used the nearly collinear setup described above, which enables the spatial separation of the pump and probe beams even when they overlap spatially inside the sample. This introduces a source of distortion in the data due to spatial walk-off between the pump and probe pulses as they travel through the

sample. To minimize this walk-off, we focused the pump and probe beams with two small lenses placed as close together as possible. In order to ensure that the walk-off did not affect the spatial resolution, we made the plane shared by the pump and probe beams perpendicular to the axis along which the pump lens was moved. We accomplished this by directing the probe beam below the pump lens and moving the relative focal position horizontally. Measurements were performed at two values of the azimuth differing by π, defining the x axis. The resolution in $z-v_g t$ is determined by the pulsewidth of the probe pulse and in x by the focal waist of the probe beam.

Ultrafast pulses were generated by a Ti:sapphire oscillator producing 800-nm, 60-fs pulses at the repetition rate of 82 MHz. Acousto-optic amplitude modulators were used to modulate the pump and probe beams at 3 MHz and 2.95 MHz, respectively, and the probe was detected with an unbiased photodiode at the difference frequency, 50 kHz, with a lock-in amplifier with time constant 30 ms. The maximum pump and probe average power at the sample was ~140 and 30 mW, respectively, limited mostly by the efficiency of the modulators. We emphasize the importance of the double-modulation technique because it helps reject the scattered pump light.

While the technique described here produces data of high quality, it is important to note that it takes hours to produce a single picture. Recently, experiments have been performed using a Zernike method with a charge-coupled-device (CCD) camera, to image the phase change of a weakly focused probe beam caused by the polariton field as a function of position and time delay.[28,43] That is a much faster technique for imaging the Cherenkov field, although it suffers from unwanted large scattering near the pump pulse.

B. Point source: Experiments

If the pump pulse is focused to a waist smaller than the wavelength of the polariton, we can approximate it as a point dipole. Because of the large thickness of our samples, we are limited to a focal waist of about 20 μm which corresponds to a maximum polariton frequency of 2–4 THz, depending on the material. For lower frequencies, the pump pulse acts like a point dipole.

First we discuss the data on $LiTaO_3$, a superluminal material; see Fig. 7. Our sample was a wafer 2 in. in diameter and 1 mm thick with orientation such that the optic axis is perpendicular to the surface normal, and we used frequency shift detection. For pulses of wavelength 800 nm, $\theta_C = 69°$. The experiment matches the calculations quite well after taking into account the 18-μm pump waist by convoluting the point dipole solution with a Gaussian of that width. However, the absence of ripples behind the sharp Cherenkov cone indicates that damping, not included in the simulation, is strong for higher frequencies. In addition to polaritons of the lowest branch, we were also able to generate and detect polaritons and coherent phonons from higher branches; see later.

Our measurements on ZnTe, a subluminal material, and the comparison with calculations are shown in Fig. 8. The

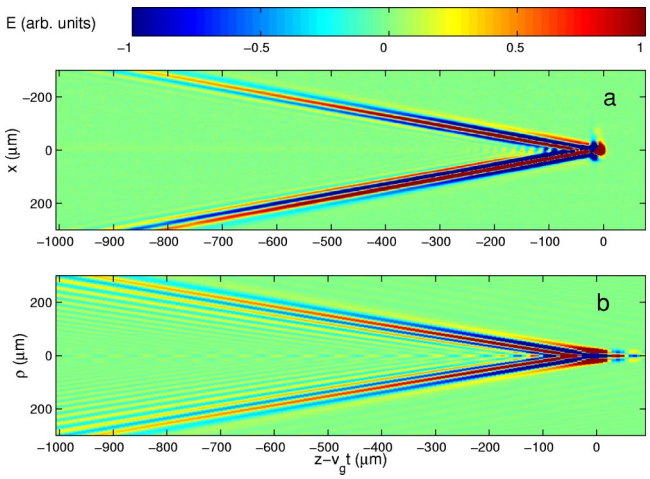

FIG. 7. (Color online) (a) Experimental results for $LiTaO_3$. The pump beam waist is 18 μm. The scan took a total of 6 h, or a little over 1 min per row. (b) Convolution of the point dipole field with a 18-μm Gaussian.

(110)-oriented ZnTe sample was $10\times10\times1$ mm^3, and polarization-sensitive detection was used. The data show many of the features predicted for subluminal CR. The artifact that appears about 1.6 ps after the pump pulse is due to a second pulse about 1000 times smaller than the pump pulse, due to a reflection from an optical element upstream. We have subtracted the contribution from an exponentially decaying signal caused by free carriers generated by two-photon absorption. This signal is partially balanced out by using polarization-sensitive detection, and the remnant has been fitted and subtracted out in Fig. 8(a) to show the absence of CR near $x=0$.

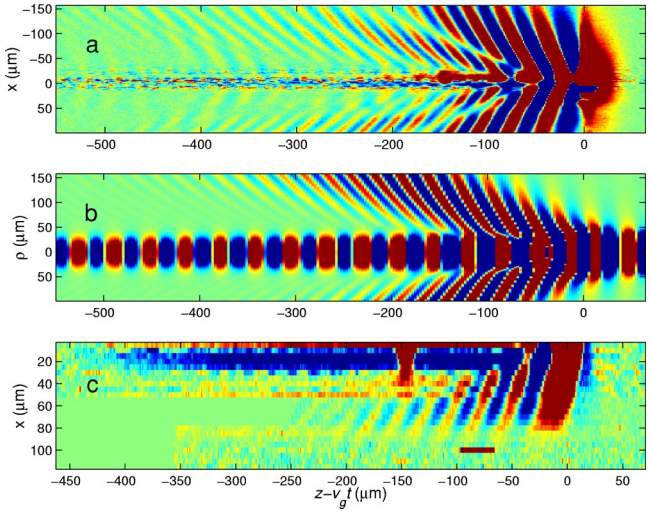

FIG. 8. (Color online) (a) Results of a pump-probe differential transmission experiment in ZnTe. An overall constant background was subtracted for each time scan, and a decaying exponential was subtracted out for time scans near $x=0$. The feature 1.6 ps behind the pump pulse is an artifact. Each row is an average of two scans, and the total acquisition time was 7 h. (b) Calculation for a point dipole convoluted with a 22-μm Gaussian in the transverse direction. (c) Experimental data for a 300-μm-thick ZnTe sample.

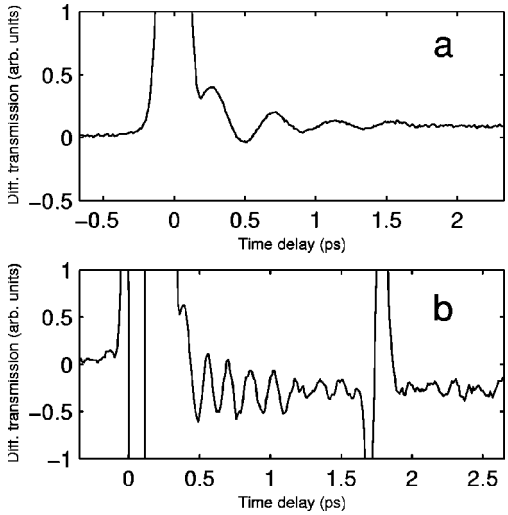

FIG. 9. Results of pump-probe experiments with weakly focused ultrafast pulses in (a) ZnTe and (b) GaP. The region near time zero is dominated by two-photon absorption. (a) 1 mm-thick ZnTe crystal. The main frequency is roughly 2 THz. (b) 1-mm-thick GaP crystal. The main frequency is roughly 7.5 THz. The feature at 1.8 ps is an artifact due to a reflected pulse.

As discussed earlier, subluminal CR is expected to exhibit a beating pattern. In Fig. 8(a), there is a striking node that separates the shock wave into two and possibly three distinct parts. This can be explained in the calculations by both subluminal beats or by a convolution artifact due to the finite spatial size of the pump and probe pulses. However, note that the node is not as prominent in the calculation. This discrepancy and the lack of experimental signal near $x=0$ are probably due to the finite size of the crystal, as discussed in detail later.

C. Planar source: Experiments

For the planar geometry, scans were performed only in the z-$v_g t$ direction. Results for GaP and ZnTe with a pump waist of roughly 100 μm are shown in Fig. 9. The GaP sample, (110) oriented, was a $4\times1\times1$ mm^3 crystal. The time scans show oscillations at the group-velocity-matched frequencies predicted by theory, with an apparent decay probably due to a combination of the finite length of the sample (see below) and the finite extent of the pump pulse.[18] The planar geometry is commonly used for generating THz pulses by nonresonant optical rectification.[27] The distortion of the electro-optic sampling signal due to infrared dispersion, especially in a thick crystal, has been the subject of much discussion recently.[44,45]

We also performed an experiment on the superluminal material $LiTaO_3$. As expected, there was no signal from the lowest polariton branch. However, our pulses were short enough to see higher branches. The phase-matching condition is given by Ω/v_g, and this expression was found to match the higher polariton branches quite well.

D. Finite-crystal effects

Point geometry experiments were also performed on a 300-μm thick ZnTe sample. As is apparent in Fig. 8(c), the node we observed in the 1-mm-thick crystal has now disappeared. This is probably a result of the breakdown of the infinite crystal approximation. In the superluminal regime, the infinite crystal calculation works well because the radiation is emitted at large angles at all frequencies down to zero. Therefore, effects of the finiteness of the crystal can be expected only at the very edge of the shock wave, at $\rho = L\tan\theta_C = Ln_0/c$, where L is the length of the crystal. For example, the edge of the shock wave is at $\rho\approx2.6$ mm in our 1-mm-thick $LiTaO_3$ sample, well beyond what we can practically measure due to the fall-off proportional to $\rho^{-1/2}$ in the electric field from a point source.

The situation is considerably different in the subluminal regime because polaritons near Ω_C are emitted in the near-forward direction. In the 1-mm-thick ZnTe crystal, the Cherenkov angle for 2.5 THz polaritons is about 9°, so that this component reaches $\rho=160$ μm before the pulse reaches the end of the crystal. In the 300 μm thick crystal, it only reaches $\rho=50$ μm. Thus, the subluminal beats, due to interference between frequency components sent in the forward direction, require some propagation time to develop. We believe this is the reason why they do not appear in the thin crystal. This could also explain the other discrepancies between theory and experiment in Fig. 8. The large oscillatory signal at Ω_C near $x=0$ in the calculation is clearly absent in the experiment, probably because radiation at Ω_C is emitted in the forward direction. The difference in the shape of the cone between theory and experiment is likely due to the same effect. A finite-crystal calculation is probably needed to fully understand the details of the experiment. Note that CR in a finite crystal is similar to the so-called ''Tamm problem'' of CR for a particle traveling along a finite path.[22,46]

The finiteness of the crystal is expected to play an even more important role in the planar geometry, in which Cherenkov components are emitted exclusively in the forward direction. The CR pattern is the result of interference among these components, so that this pattern should change dramatically with crystal thickness. A very thin crystal would show no propagation effects, simply reproducing the time derivative of the pump pulse envelope as a short THz pulse.

E. Periodic source: Experiments

We adapted the setup described previously to perform experiments with two pump pulses, creating a periodic dipolar distribution in $LiTaO_3$, and used frequency shift detection to map the polariton field. The pump pulse was split into two equally intense pulses which were focused by a single lens and crossed inside the sample at an angle α. Using a beam waist such that $w\ll v_g\tau/\sin\alpha$, we avoided the so-called ''pancake effect,''[30] a shrinking of the overlap between weakly focused pulses due to their short duration. In our experiments, we did not have to measure α, because the grating period was directly obtained by measuring the coherent artifact as a function of spatial position. As for the point geometry, we mapped the polariton field due to this pump configuration as a function of $z-v_g t$ and x. The results in Fig. 10 show excellent agreement with the theoretical predictions.

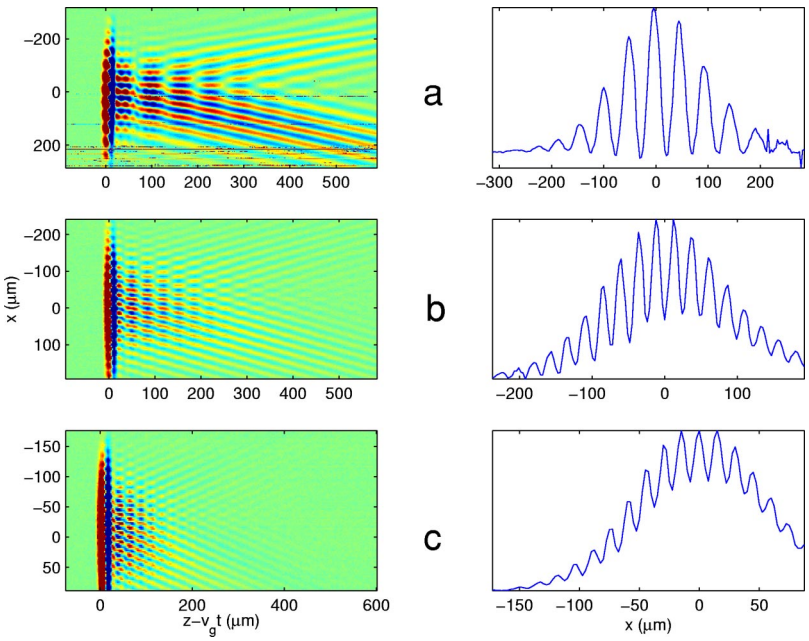

FIG. 10. (Color online) Results of transient-grating experiments in $LiTaO_3$. Left: derivative of the polariton field as a function of time delay and position of the pump lens. Right: cross sections at zero time delay, showing the intensity grating's period. The phase-matched frequency is (a) 1 THz, (b) 2 THz, and (c) 3 THz. Damping is higher at higher polariton frequencies.

F. $LiTaO_3$: Phonons and Polaritons

$LiTaO_3$ has a particularly rich history in the ISRS literature.[10,11,28,30,43,47–52] In this section we compare our data to those of other reports. There are two main points of contention in the literature: the origin of frequency-dependent damping effects and avoided crossings at low frequency. Our results for the polariton dispersion are summarized in Fig. 11.

As previously discussed for the transient-grating geometry [see below Eq. (17)], the Cherenkov angle appears in the expression for the polariton wave vector. Using the correct expression, our data fall almost exactly on the dispersion relation of the lowest branch A_1 polaritons inferred from the IR data of Barker *et al.*[35] Recent ISRS papers have begun to take this into account as well.[30,31] The grating technique is also sensitive to nondispersive phonons, and the signal at 7.8 THz roughly matches an A_1 phonon peak seen in Raman spectra.[39] Scans in the planar geometry, with wave vector given by the group velocity of the pulse, are also shown in Fig. 11. Here, we are sensitive to even more phonon branches, including a higher-branch polariton above 12 THz. Note that higher branches were also observed in a recent heterodyne experiment.[30]

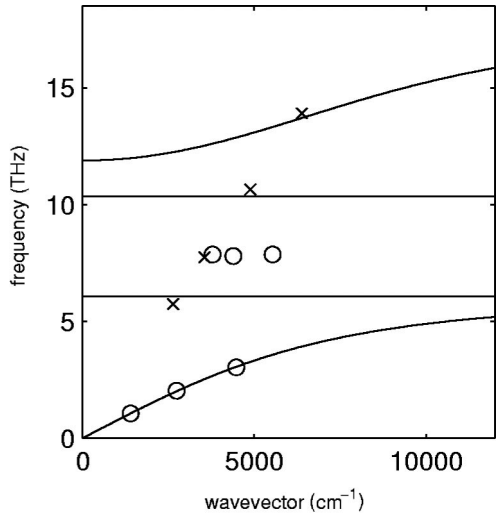

FIG. 11. Summary of results in $LiTaO_3$. Circles indicate frequencies measured using the grating technique, with wave vector given by $k_x/\sin\theta$, where k_x is the wave vector of the grating and θ is the Cherenkov angle. Crosses indicate measurements with a planar geometry, with wave vector given by Ω/v_g. The solid lines give the polariton dispersion according to the infrared measurements of Ref. 35.

Our measurements of the polariton damping rate γ by the grating method,[53] agree very well with those reported by others: $\gamma=2.4\ \mathrm{cm}^{-1}$ at 1 THz, $\gamma=4.4\ \mathrm{cm}^{-1}$ at 2 THz, and $\gamma=7.5\ \mathrm{cm}^{-1}$ at 3 THz. Large damping, peaked at 2.7 THz, was reported by Auston and Nuss in their original experiment.[16] They suggested that this was due to multiphonon absorption. In their homodyne transient grating experiment, Wiederrecht *et al.*[10] measured increased damping peaked at 2.76 THz and 4.38 THz, and attributed this to strain-induced coupling to heavily damped *E*-symmetry modes at the same frequencies. Very recently, Crimmins, Stoyanov, and Nelson measured the damping rate using heterodyne detection and suggested that the damping is due to quadratic coupling between the phonon-polariton mode at 2.1 THz and the lowest-lying *E* mode at 4.2 THz.[30]

The inelastic neutron scattering data of Cheng *et al.*[54] support the idea that the damping is due to anharmonicity—more precisely, to a process involving the simultaneous creation and destruction of two different phonons. Close to the observed peaks at 2.76 and 4.38 THz, the phonon dispersion shows TO and LA (TA) branches for which the frequency difference at the zone edge, where the density of states is large, is 2.6 THz (4 THz). In this context, we note that decay by two-phonon difference modes has been seen in many materials, including ZnTe.[55] Furthermore, many spontaneous

Raman studies,[39,56] including one on our particular crystal,[57] show a broad peak centered at 2.55 THz, consistent with a second-order feature. An alternative explanation for polariton broadening, supported by the fact that the TA and LA branches at the zone edge are at 3.2 and 4.6 THz, respectively,[54] is coupling to high-wave-vector phonons due to disorder-induced breakdown of momentum conservation. Given that $LiTaO_3$ is often nonstoichiometric, defect-related processes may contribute strongly to the damping.

Another anomaly reported in $LiTaO_3$ is an extra avoided crossing in the polariton dispersion at 0.9 THz.[11,47,48] Similar avoided crossings were also reported for $LiNbO_3$,[58] and increased absorption was observed at the corresponding frequencies in stimulated Raman gain measurements.[59] The avoided crossings were assigned by Bakker and co-workers[11] to quantum beats between levels of an intrinsic anharmonic potential. However, our work on $LiTaO_3$, as well as a recent heterodyne ISRS experiment,[30] shows no sign of an avoided crossing at 0.9 THz. The observation of several low-lying modes in a CARS study of MgO-doped $LiNbO_3$ (Ref. 60) suggests that the extra modes are due to defects. If this were the case, the reported discrepancies for $LiTaO_3$ may simply be due to differences in the concentration of defects for different samples.

We take issue with the intrinsic anharmonicity proposed by Bakker *et al.*[11] to explain these extra modes. Unlike in molecules, lattice anharmonicity in solids leads to decay, because anharmonic coupling involves a continuum of modes. Hence, unless the anharmonicity is strong enough to support two-phonon bound states, it cannot introduce new frequencies. To the best of our knowledge, no such bound states have been observed in $LiTaO_3$ or $LiNbO_3$.

An unexplored area is the role of anisotropy in $LiTaO_3$. As briefly discussed earlier, for frequencies approaching the lowest *E*-phonon frequency, the index of refraction becomes increasingly anisotropic. Anisotropy is known to have an important effect on CR,[23] but as far as we know, it has been completely ignored in the $LiTaO_3$ literature. For a point charge traveling through a uniaxial material in a direction perpendicular to the optical axis, both ordinary and extraordinary waves are emitted, with the extraordinary waves polarized at a finite angle to the optical axis. Assuming that this is also true for a dipole oriented along the optic axis, it should have a large effect on the CR pattern.

VII. CONCLUSIONS

In summary, we have used ultrafast optical pulses to generate and image coherent polariton fields in ZnTe, GaP, and $LiTaO_3$. For single and multiple pulses of arbitrary shape and, in particular, for the transient-grating geometry, we have shown that the polariton field can be calculated by convolving the slowly varying pulse envelope with the Cherenkov field due to a dipole. The standard phase-matching arguments can also be explained by applying ideas from the theory of Cherenkov radiation. Results for pointlike and planar sources reveal important differences between the superluminal and subluminal regimes, especially for the Cherenkov emission by a plane of dipoles which can only occur in the subluminal case.

ACKNOWLEDGMENTS

We thank G. Narayanasamy for assistance in the early stages of the experiments and T. E. Stevens for useful discussions. We are grateful to M. DeCamp, C. Herne, and J. Murray for providing the ZnTe samples and J. Deibel for the $LiTaO_3$ sample. This work was supported by the AFOSR under Contract No. F49620-00-1-0328 through the MURI program and by the NSF FOCUS Physics Frontier Center.

[1] M. Born and K. Huang, *Dynamical Theory of Crystal Lattices* (Oxford University Press, Oxford, 1954).
[2] D.L. Mills and E. Burstein, Rep. Prog. Phys. **37**, 817 (1974).
[3] C.H. Henry and J.J. Hopfield, Phys. Rev. Lett. **15**, 964 (1965).
[4] W.L. Faust and C.H. Henry, Phys. Rev. Lett. **17**, 1265 (1966).
[5] Y.R. Shen and N. Bloembergen, Phys. Rev. **137**, A1787 (1965).
[6] G.M. Gale, F. Vallee, and C. Flytzanis, Phys. Rev. Lett. **57**, 1867 (1986).
[7] Y.-X. Yan and K.A. Nelson, J. Chem. Phys. **87**, 6240 (1987).
[8] L. Dhar, J.A. Rogers, and K.A. Nelson, Chem. Rev. (Washington, D.C.) **94**, 157 (1994).
[9] R. Merlin, Solid State Commun. **102**, 207 (1997).
[10] G.P. Wiederrecht, T.P. Dougherty, L. Dhar, K.A. Nelson, D.E. Leaird, and A.M. Weiner, Phys. Rev. B **51**, 916 (1995).
[11] H.J. Bakker, S. Hunsche, and H. Kurz, Rev. Mod. Phys. **70**, 523 (1998).
[12] M. Bass, P.A. Franken, J.F. Ward, and G. Weinreich, Phys. Rev. Lett. **9**, 446 (1962).
[13] P.K. Tien, R. Ulrich, and R.J. Martin, Appl. Phys. Lett. **17**, 447 (1970).
[14] D.H. Auston, K.P. Cheung, J.A. Valdmanis, and D.A. Kleinman, Phys. Rev. Lett. **53**, 1555 (1984).
[15] D.A. Kleinman and D.H. Auston, IEEE J. Quantum Electron. **20**, 964 (1984).
[16] D.H. Auston and M.C. Nuss, IEEE J. Quantum Electron. **24**, 184 (1988).
[17] B.B. Hu, X.-C. Zhang, D.H. Auston, and P.R. Smith, Appl. Phys. Lett. **56**, 506 (1990).
[18] T.E. Stevens, J.K. Wahlstrand, J. Kuhl, and R. Merlin, Science **291**, 626 (2001).
[19] J.K. Wahlstrand, T.E. Stevens, J. Kuhl, and R. Merlin, Physica B **316–317**, 55 (2002).
[20] G.N. Afanasiev, V.G. Kartavenko, and E.N. Magar, Physica B **269**, 95 (1999).
[21] I. Frank and I. Tamm, Dokl. Akad. Nauk SSSR **14**, 109 (1937).
[22] I. Tamm, J. Phys. (Moscow) **1**, 439 (1939).
[23] V.P. Zrelov, *Cherenkov Radiation in High-Energy Physics* (Israel Program for Scientific Translation, Coronet Books, 1970).
[24] T.E. Stevens, J. Kuhl, and R. Merlin, Phys. Rev. B **65**, 144304 (2002).

[25] Our use of the terms superluminal and subluminal has been recently criticized [V.L. Ginzburg, Phys. Usp. **45**, 341 (2002)]. However, we believe that it is important to draw such a strong distinction between the two qualitatively different regimes, especially for nonlinear optics applications.
[26] Q. Wu and X.-C. Zhang, Appl. Phys. Lett. **68**, 1604 (1996).
[27] A. Nahata, A.S. Weling, and T.F. Heinz, Appl. Phys. Lett. **69**, 2321 (1996).
[28] R.M. Koehl, S. Adachi, and K.A. Nelson, J. Chem. Phys. **110**, 1317 (1999).
[29] C.A. Gautier, J.C. Loulergue, and J. Etchepare, Solid State Commun. **100**, 133 (1996).
[30] T.F. Crimmins, N.S. Stoyanov, and K.A. Nelson, J. Chem. Phys. **117**, 2882 (2002).
[31] J. Hebling, Phys. Rev. B **65**, 092301 (2002).
[32] J. Hebling, G. Almasi, I.Z. Kozma, and J. Kuhl, Opt. Express **10**, 1161 (2002).
[33] A. Mooradian and G.B. Wright, Solid State Commun. **4**, 431 (1966).
[34] G. Gallot, J. Zhang, R.W. McGowan, T.-I. Jeon, and D. Grischkowsky, Appl. Phys. Lett. **74**, 3450 (1999).
[35] A.S.J. Barker, A.A. Ballman, and J.A. Ditzenberger, Phys. Rev. B **2**, 4233 (1970).
[36] A.N. Pikhtin, V.T. Prokopenko, and A.D. Yas'kov, Sov. Phys. Semicond. **10**, 1224 (1976).
[37] D.T.F. Marple, J. Appl. Phys. **35**, 539 (1964).
[38] A. Leitenstorfer, S. Hunsche, J. Shah, M.C. Nuss, and W.H. Knox, Appl. Phys. Lett. **74**, 1516 (1999).
[39] C. Raptis, Phys. Rev. B **38**, 10 007 (1988).
[40] O. Albert, M. Duijser, J.C. Loulergue, and J. Etchepare, J. Opt. Soc. Am. B **13**, 29 (1996).
[41] G.D. Boyd and M.A. Pollack, Phys. Rev. B **7**, 5345 (1973).
[42] J.A. Valdmanis, G. Mourou, and C.W. Gabel, Appl. Phys. Lett. **41**, 211 (1982).
[43] R.M. Koehl and K.A. Nelson, J. Chem. Phys. **114**, 1443 (2001).
[44] H.J. Bakker, G.C. Cho, H. Kurz, Q. Wu, and X.-C. Zhang, J. Opt. Soc. Am. B **15**, 1795 (1998).
[45] G. Gallot and D. Grischkowsky, J. Opt. Soc. Am. B **16**, 1204 (1999).
[46] G.N. Afanasiev, V.G. Kartavenko, and J. Ruzicka, J. Phys. A **33**, 7585 (2000).
[47] H.J. Bakker, S. Hunche, and H. Kurz, Phys. Rev. Lett. **69**, 2823 (1992).
[48] H.J. Bakker, S. Hunsche, and H. Kurz, Phys. Rev. B **48**, 13 524 (1993).
[49] C.J. Brennan and K.A. Nelson, J. Chem. Phys. **107**, 9691 (1997).
[50] H.M. Perry and T.P. Dougherty, Phys. Rev. B **55**, 5778 (1997).
[51] H. Bakker, Phys. Rev. B **57**, 3167 (1998).
[52] V. Romero-Rochin, R.M. Koehl, C.J. Brennan, and K.A. Nelson, J. Chem. Phys. **111**, 3559 (1999).
[53] Due to the complexity of the Cherenkov field pattern, extreme care must be taken in extracting damping from ISRS data. The values quoted are from measurements using a large transient grating, in which case spurious edge effects are minimized.
[54] G. Cheng, B. Hennion, P. Launois, M. Xianlin, X. Binchao, and J. Yimin, J. Phys.: Condens. Matter **5**, 2707 (1993).
[55] M. Schall, M. Walther, and P. Uhd Jepsen, Phys. Rev. B **64**, 094301 (2001).
[56] A.F. Penna, A. Chaves, P.d.R. Andrade, and S.P.S. Porto, Phys. Rev. B **13**, 4907 (1976).
[57] J. K. Wahlstrand and R. Merlin (unpublished).
[58] H.J. Bakker, S. Hunsche, and H. Kurz, Phys. Rev. B **50**, 914 (1994).
[59] T. Qiu, T. Tillert, and M. Maier, Opt. Commun. **119**, 149 (1995).
[60] U.T. Schwarz and M. Maier, Phys. Rev. B **58**, 766 (1998).